Diazapentacene Derivatives as Thin-Film Transistor Materials: Morphology Control in Realizing High-Field-Effect Mobility

Shou-Zheng Weng,[†] Paritosh Shukla,[†] Ming-Yu Kuo,[†] Yu-Chang Chang,[†] Hwo-Shuenn Sheu,[‡] Ito Chao,*[,†] and Yu-Tai Tao*[,†]

Institute of Chemistry, Academia Sinica, Taipei 115, Taiwan, Republic of China, and National Synchrotron Radiation Research Center, Hsinchu 300, Taiwan, Republic of China

ABSTRACT 5,7,12,14-Tetrachloro-6,13-diaza-6,13-dihydropentacene (TCDAHP) and 5,7,12,14-tetrachloro-6,13-diazapentacene (TCDAP) were synthesized and assessed as the active channel materials for thin-film transistor applications. Analyses of the crystal structures of these molecules revealed that both exhibited slipped $\pi-\pi$ stacking of the long and fused aromatic moiety. Although the packing features of the two compounds are basically identical, their highest occupied molecular orbitals, which are relevant to hole transport, are very different. Better mobility was predicted for TCDAHP over TCDAP based on the dimeric structure in the X-ray coordinates. The morphologies of thin films of TCDAHP and TCDAP prepared by thermal evaporation depend critically on the substrate on which the molecules were deposited: from the amorphous state on a SiO_2/Si surface to the crystalline state on a pentacene buffer layer surface. The performance of thin-film transistors prepared on various substrate surfaces was studied. While no field-effect mobility was observed for these films deposited on SiO_2/Si, a high mobility of 1.4 cm^2/(V s) for the TCDAHP film was achieved when deposited on a pentacene buffer layer prepared on a rubbed monolayer of *n*-nonyltrichlorosilane on a SiO_2/Si surface. A similar device prepared from TCDAP gave a mobility of 0.13 cm^2/(V s).

KEYWORDS: organic thin-film transistor • diazapentacenes • induced crystallization • pentacene • film morphology

INTRODUCTION

Electronic and optoelectronic devices based mainly on organic materials, such as organic light-emitting diodes (OLEDs), organic field-effect transistors (OFETs), and organic photovoltaics, are making their way into our daily lives (1). The use of organic-based materials in electronics also enables the exciting new technology of flexible electronics (2). OFET will play a major role in many of these organic electronic devices as the driving components of electric circuits. One of the major obstacles for the wide application of OFETs is the relatively low field-effect mobility attainable from organic materials compared with that from inorganic semiconductors. Nevertheless, rapid progress has been made over the past decade so that a mobility comparable to that of amorphous silicon has been realized. Such a mobility is enough for many low-end product applications.

The performance of an OFET is determined by a number of factors, including the intrinsic molecular/electronic structure, crystal packing, film morphology, material stability, etc. These factors are, nevertheless, all related to the molecular structure such that a modification in the molecular structure may influence all of the above-mentioned characteristics, making the structure−device property correlation complicated. Pentacene is one of the most studied molecules because of its high mobility. The mobility in the thin-film state under specific fabrication conditions can approach 3−5 cm^2/(V s) (3). However, besides the low-solubility problem, it has stability issues due to photooxidation or dimerization via a Diels−Alder reaction (4). A lot of effort has been devoted to further improve the mobility, stability, or solubility by modifying the pentacene framework (5). On the other hand, nitrogen-containing oligoacenes, in which some of the acene C−H groups are replaced with sp^2-hybridized nitrogen atoms (=N−), have been shown both experimentally (6) and theoretically (7) to be featured with a less negative reductive potential (6), high electron affinity (EA) (6, 7), and ambient stability (6). Nitrogen-containing oligoacenes can even afford opportunities to form a self-complemented 2D layer through the abundant C−H···N short contacts so as to give the cofacial packing arrangement in contrast to the herringbone arrangement, which is typical for pentacene (7a, 8). Furthermore, Nuckolls et al. demonstrated that the incorporation of *N*,*N*-dihydrodiaza moieties (i.e., the sp^3-hybridized −NH− fragment) into one of the rings largely improves the stability of pentacene because of the interruption of the π-conjugation framework of pentacene (9). More recently, diazatetracene, *N*,*N*-dihydrodiazatetracene, and two dialkynylated derivatives were synthesized (6a) and assessed for transistor application (10). Both diazatetracene and *N*,*N*-dihydrodiazatetracene are stable compounds. Nevertheless, while *N*,*N*-dihydrodiazatetracene is stable (6a), its dialkynylated *N*,*N*-dihydrodiazatetracene derivatives tend to be oxidized quickly to dialkynylated diazatetracenes.

* E-mail: ytt@chem.sinica.edu.tw (Y.-T.T.), ichao@chem.sinica.edu.tw (I.C.).
Received for review June 27, 2009 and accepted August 26, 2009
[†] Academia Sinica.
[‡] National Synchrotron Radiation Research Center.
DOI: 10.1021/am9004418

Scheme 1[a]

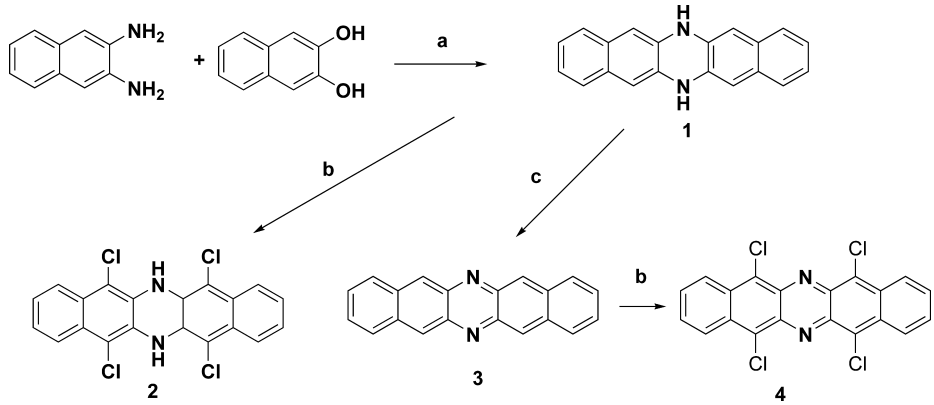

[a] Reagents and conditions: (a) 200 °C; (b) SO_2Cl_2 in CCl_4, 80 °C; (c) $Cu(OAc)_2 \cdot H_2O$ in pyridine, air, 70 °C.

At a molecular level, two factors, the electronic coupling between molecules and the reorganization energy during charge transport, are considered to be important for charge transport in organic semiconductors (11). For electronic coupling (t), it has been pointed out that the cofacial $\pi-\pi$ stacking can provide more effective orbital overlap and thus higher electronic coupling that facilitates carrier hopping between molecules (12). Previously, Sarma and Desiraju reported that halogen groups facilitate $\pi-\pi$ stacking of an aromatic system (13). Bao et al. used dichloro substitution to alter the herringbone packing of tetracene to $\pi-\pi$ stacking, resulting in an improved mobility (14). For the already π-stacked triphenylene, it has been predicted theoretically that the presence of nitrogen atoms in hexaazatriphenylene has a favorable impact on the electronic coupling for hole transport in the triphenylene systems (15). As for the reorganization energy, strategies of molecular design to minimize the impact of chemical modifications on the internal reorganization energy (λ) have been proposed (7b, 16). It was shown that replacing five carbon atoms in pentacene with sp^2-hybridized nitrogen atoms or attaching several chlorine atoms to pentacene increases λ by less than 0.1 eV (7). In view of the merits mentioned above in terms of the reorganization energy, crystal engineering, and stability, we find pentacene analogues with nitrogen and chlorine substitutions attractive candidates for OFET materials.

Finally, another crucial factor, particularly in the case of thin-film transistor applications, is the morphology of the deposited organic film (17, 18). Films deposited at different substrate temperatures could have drastically different mobilities, as a result of different phases (17) or grain sizes involved (18). Much improvement in the mobility was also observed on differently treated surfaces (19), again as a result of the different morphologies. Thus, controlling the size, connectivity, and orientation of the crystalline grains in a film can be vital to the ultimate mobility that can be observed.

In this paper, we combine the strategies of chlorination, diaza, and *N*,*N*-dihydrodiaza substitution in the pentacene molecule in order to promote the $\pi-\pi$ stacking of the conjugate framework and report the synthesis and characterization of a new semiconducting molecule, 5,7,12,14-tetrachloro-6,13-diaza-6,13-dihydropentacene (TCDAHP), as well its planar analogue, 5,7,12,14-tetrachloro-6,13-diazapentacene (TCDAP), as the channel material for FET purposes. While the field-effect mobility for TCDAHP was predicted to be superior to that of TCDAP based on the single-crystal structures, the measured p-channel mobility for the thin-film configuration is very much constrained by the film morphology upon deposition. We successfully achieved a high mobility of 1.4 $cm^2/(V\ s)$ for a deposited TCDAHP thin film when using a pentacene buffer layer prepared on a rubbed monolayer of *n*-nonyltrichlorosilane (NTS) on a SiO_2/Si substrate. The improvement in the mobility originates from improved crystallinity and connectivity of the grains in the film, as a result of favorable molecular−substrate interaction. Under similar fabrication conditions, a mobility of 0.13 $cm^2/(V\ s)$ was measured for TCDAP.

RESULTS AND DISCUSSION

Synthesis. The syntheses of TCDAHP (**2**) and TCDAP (**4**) are outlined in Scheme 1. Condensation of 2,3-diaminonaphthalene with 2,3-dihydroxynaphthalene gave 6,13-diaza-6,13-dihydropentacene (**1**). Direct chlorination with SO_2Cl_2 was carried out in carbon tetrachloride to give the desired compound **2**. For TCDAP, oxidation of the diazadihydro derivative **1** was carried out with cupric acetate before the chlorination reaction. Both compounds were purified by temperature-gradient sublimation and characterized by NMR, mass, and elemental analysis. Thermogravimetric analyses show that both TCDAHP and TCDAP decompose above 350 °C.

Crystal Structure and Theoretical Calculation. Single crystals of TCDAP were obtained by the vapor-phase-transfer method in a temperature-gradient tube. For TCDAHP, vapor-phase transfer under an argon flow resulted in partial degradation to TCDAP. Thus, the crystallites were obtained by chain sublimation under a vacuum. Both gave long needlelike morphology. X-ray analyses showed a monoclinic structure with a $P2_1/n$ space group for both compounds. Figure 1 shows the molecular packing, and the crystal parameters are reported in Table 1. In the presence of chlorine and nitrogen atoms, both compounds give a shifted $\pi-\pi$ stacking as expected rather than the herringbone

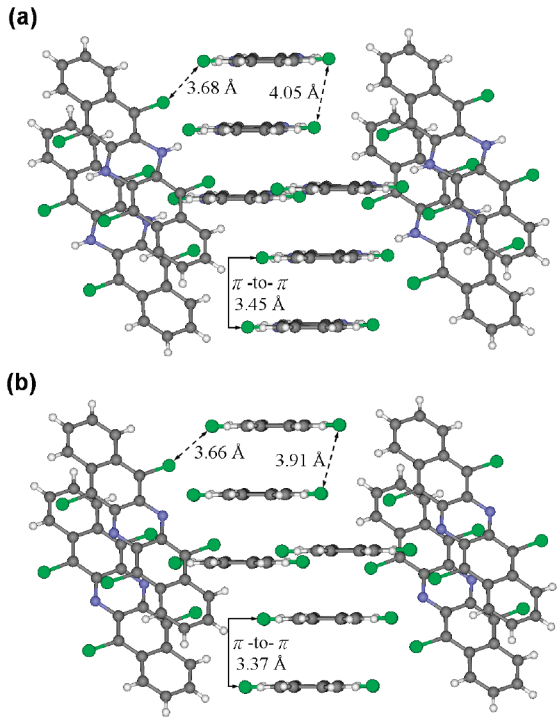

FIGURE 1. Molecular packing of (a) TCDAHP and (b) TCDAP.

Table 1. Lattice Parameters of TCDAHP and TCDAP[a]

compound	*a* (Å)	*b* (Å)	*c* (Å)	*β* (deg)	space group
TCDAHP	4.05	12.13	17.11	90.97	$P2_1/n$
TCDAP	3.91	12.15	16.95	94.77	$P2_1/n$

[a] Room temperature. $\alpha = \gamma = 90°$.

arrangement. Short π–π distances of 3.45 and 3.37 Å are observed for TCDAHP and TCDAP, respectively. The pentafused ring shifts by one ring between layers so that one of the two chlorine atoms in the upper layer fall between the two chlorine atoms in the lower layer. The distances between adjacent chlorine atoms are in the range of 3.66–4.05 Å. From the viewpoint of nonbonded interactions, the diazadihydro and diaza groups are very different; one bears hydrogen-bond donors (N–H), while the other bears hydrogen-bond acceptors (N). Because the diazadihydro and diaza substituents do not influence the molecular packing of these two compounds, the similar structural motifs in crystal the structures of TCDAHP and TCDAP must be steered by the chlorine atoms.

For hole transportation, the calculated values of the reorganization energy (λ^+) and electronic coupling (t^+) between the highest occupied molecular orbitals (HOMOs) are shown in Table 2. The ionization potential (IP) of TCDAP (6.724 eV) is close to that of perfluoropentacene (IP = 6.602 eV; λ^+ = 222 meV) (16a), but in accordance with our proposed strategies of employing chlorine and sp^2-hybridized nitrogen atoms to minimize the impact of chemical modifications on λ (7b), λ^+ (129 meV) of TCDAP is much closer to that of pentacene (IP = 5.899 eV; λ^+ = 94 meV) (16a) rather than to that of perfluoropentacene. λ^+ of TCDAHP is larger than that of TCDAP by 33 meV. The

Table 2. Internal Reorganization Energies of the Hole Transport (λ^+) and Adiabatic IPs Calculated at the B3LYP/6-31G Level[a]**

compound	λ^+ (meV)	IP (eV)	*R* (Å)	t^+ (meV)	μ^+ [cm^2/(V s)]
TCDAHP	162	6.482	4.05	123	4.16
TCDAP	129	6.724	3.91	32	0.40

[a] The distances between molecular centers (*R*), electronic couplings (t^+) of HOMOs, and hole mobilities (μ^+) are also given.

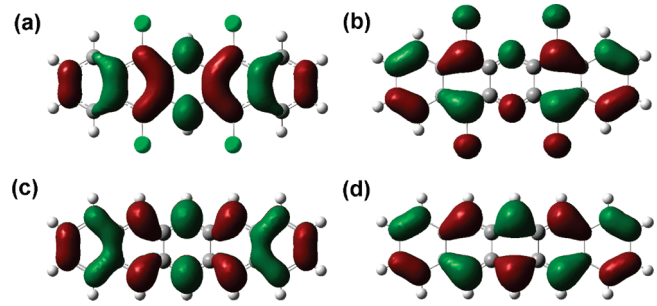

FIGURE 2. (a) HOMO of TCDAHP, (b) HOMO of TCDAP, (c) LUMO of pentacene, and (d) HOMO of pentacene.

smaller λ^+ of TCDAP is consistent with the nonbonding feature of the central ring of the HOMO of TCDAP (Figure 2b). Owing to the nonbonding feature, when an electron is taken out of TCDAP, the changes of the bond lengths (C–C and C–N) in the central ring are no more than 0.002 Å. The antibonding feature of the central ring of the HOMO of TCDAHP (Figure 2a), on the other hand, has resulted in changes of the bond lengths as large as 0.012 Å in the same region. In other words, for TCDAHP, all rings contribute to the reorganization energy upon removal of an electron, but for TCDAP, one ring is basically exempted.

t^+ is calculated based on the dimer along the direction of π–π stacking, as shown in Figure 1. The results show that t^+ for TCDAHP (123 meV) is significantly larger than that for TCDAP (32 meV), even though the π–π distance is slightly shorter for TCDAP. Previously, Brédas et al. studied the effect of relative shifts along the molecular axes on the magnitudes of electronic coupling between acene dimers (20). They showed that coupling between frontier orbitals of cofacial dimers could be oscillatory because of existence of nodal planes; even zero coupling is possible. Because HOMOs of TCDAHP and TCDAP resemble the LUMO and HOMO of pentacene, respectively (Figure 2), we looked into the electronic couplings between pentacene dimers (20) for insight of the large difference between t^+'s of TCDAHP and TCDAP. When shifted, pentacene has a local maximal electronic coupling between the LUMOs at a shift of 2.0 Å and a local minimal value between the HOMOs at a shift of 1.5 Å along the long molecular axis with a fixed π–π distance. As dimers of TCDAHP and TCDAP slipped along their long molecular axes for ca. 1.9 and 1.7 Å, respectively, these facts may be relevant to why the electronic coupling between the HOMOs (t^+) of TCDAHP is significantly larger than that of TCDAP. Moreover, both TCDAHP and TCDAP show shifts along short molecular axes (0.80 and 0.95 Å, respectively). The additional nodal plane in the HOMO along the long molecular axis of TCDAP (Figure 2b) compared to that of TCDAHP

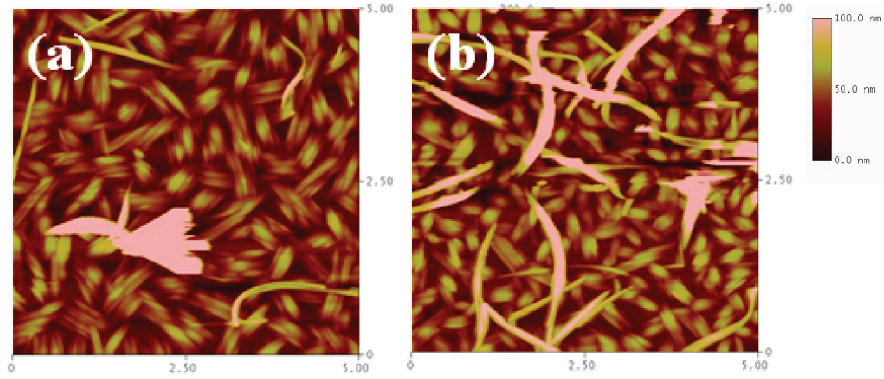

FIGURE 3. AFM micrographs of a 45 nm TCDAHP film on (a) NTS/SiO_2/Si and (b) r-NTS/SiO_2/Si surfaces.

(Figure 2a) may also play a role in its small electronic coupling. On the basis of the hopping mechanism, one can calculate the hole mobility (μ^+) with the calculated λ^+ and t^+ (21). (see the computational details.) The results show that μ^+ of TCDAHP is an order of magnitude larger than that of TCDAP. The calculated mobility of 4.16 cm/(V s) for TCDAHP is somewhat lower than that of pentacene in the D2 direction (5.43 cm^2/(V s)) but nearly 2 times higher than that in the D1 and D3 directions (21b). The above simple evaluation of mobility based on X-ray coordinates ignores the environmental impact on the reorganization energy and may not be completely transferable to thin-film mobility because the packing structure in the thin film may not be identical with that in the crystal. Nevertheless, it clearly demonstrates that, even if TCDAHP and TCDAP have closely resembled packing structures, the fundamental difference in the HOMO may lead to quite different hole-transporting properties.

Thin-Film Structure and Transistor Characterization. Thin films of TCDAHP were deposited on various substrates at a substrate temperature of 55 °C and characterized by powder X-ray diffraction (XRD) and atomic force microscopy (AFM). On the SiO_2/Si surface, only an amorphous film was obtained with no diffraction peak detectable for the film. Attempts of AFM measurements yielded poor-quality images because the molecules appeared to adhere to the AFM probe. No field-effect mobility could be measured for a device based on such a film. Films were also deposited on an NTS-monolayer-covered SiO_2/Si substrate (designated as NTS/SiO_2/Si). NTS is chosen as the surface modifier of the SiO_2 dielectric because it was shown to be advantageous over *n*-octadecyltrichlorosilane in promoting larger grains (19, 22). Previous work has demonstrated that the rubbing of a monolayer of NTS on SiO_2 promotes the formation of larger and better connected grains of pentacene (19). The improvement in the morphology was suggested to be due to fewer nucleation sites and more oriented growth on the rubbed monolayer surface. Figure 3 shows the AFM micrographs of a TCDAHP film deposited on a NTS/SiO_2/Si surface and the NTS/SiO_2/Si surface prerubbed with a flannel cloth (designated as r-NTS/SiO_2/Si). On the NTS/SiO_2/Si surface, the TCDAHP film gave morphologies of bundled grains (Figure 3a), with grain sizes of around 0.5 μm in length and a few tenths of a micrometer in width. However, little or no diffraction peak was observed in the XRD. Film deposited on rubbed r-NTS/SiO_2/Si exhibited similar morphologies, with a slight improvement in the film crystallinity, as revealed by powder XRD. The mobilities of FET devices based on these films were observable but were less than 10^{-6} cm^2/(V s).

Recently, it has been shown that a buffer layer of pentacene can induce the formation of crystalline films of rubrene and C_{60}, which tend to give amorphous films by thermal evaporation (23). We also showed that if the pentacene film has in-plane orientation, as prepared on a rubbed poly(vinyl alcohol) surface, the rubrene film deposited on the top of the pentacene buffer layer will also be oriented (24). In conjunction with our previous work that pentacene deposited on a rubbed self-assembled monolayer of NTS gave larger grains exhibiting enhanced and anisotropic mobility, we decided to insert a 3 nm pentacene buffer layer between TCDAHP and the NTS monolayer on SiO_2/Si. Control FET devices with 1.5, 3, 6, and 10 nm pentacene films showed no transistor behavior with films of 3 nm and thinner. A 6 nm film gave irreproducible mobility up to 10^{-4} cm^2/(V s). With 10 nm pentacene, reproducible mobility of 10^{-2} cm/(V s) was observed. AFM showed that, at 3 nm thickness, disconnected pentacene islands with terraces up to four or five layers were obtained. TCDAHP was deposited on a 3 nm pentacene buffer layer in the same vacuum. As shown in Figure 4a, at low thickness (5 nm) of TCDAHP, the pentacene underlayer exhibited disconnected and terraced islands, whereas TCDAHP formed streaks or rodlike grains. Figure 4b shows the AFM micrograph of 5 nm TCDAHP deposited on 3 nm pentacene that was deposited on r-NTS/SiO_2/Si. The underlying pentacene layer had larger but still disconnected grains, and the streaks or rods of TCDAHP are also larger. At a thicker film of 45 nm, long and large grains of several micrometers in length and a few tenths of a micrometer in width were formed. These long grains apparently bridged over the disconnected grains of the pentacene buffer layer, which span a submicrometer range. The long-grain morphology was related to the growth pattern of this molecule, as was also revealed by the needlelike single crystals obtained from vapor-phase transport. Improved crystallinity was indicated by the XRD patterns shown in Figure 5. A diffraction peak at $2\theta = 10.47°$ of greater intensity was observed for a film deposited on r-NTS/SiO_2/Si. Also appearing was the peak at $2\theta = 21.06°$. These peaks

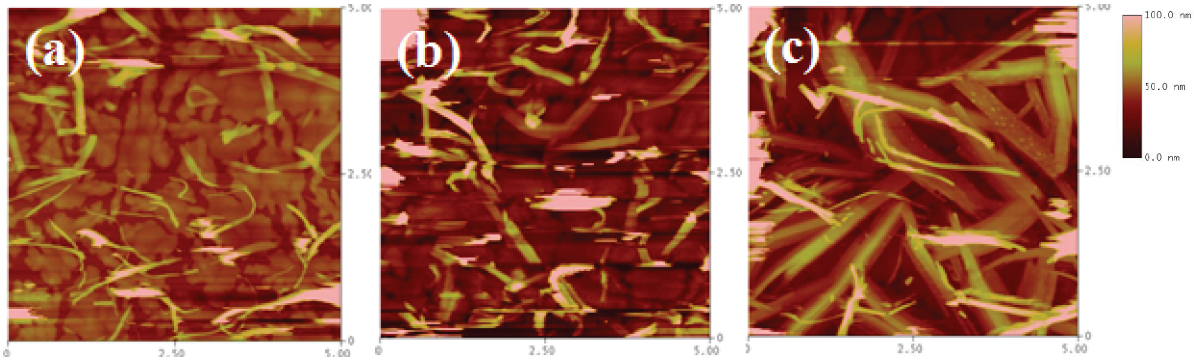

FIGURE 4. AFM micrographs of (a) 5 nm TCDAHP deposited on a 3 nm pentacene/NTS-SiO_2/Si surface, (b) 5 nm TCDAHP on a 3 nm pentacene/r-NTS-SiO_2/Si surface, and (c) 45 nm TCDAHP on a 3 nm pentacene/r-NTS-SiO_2/Si surface.

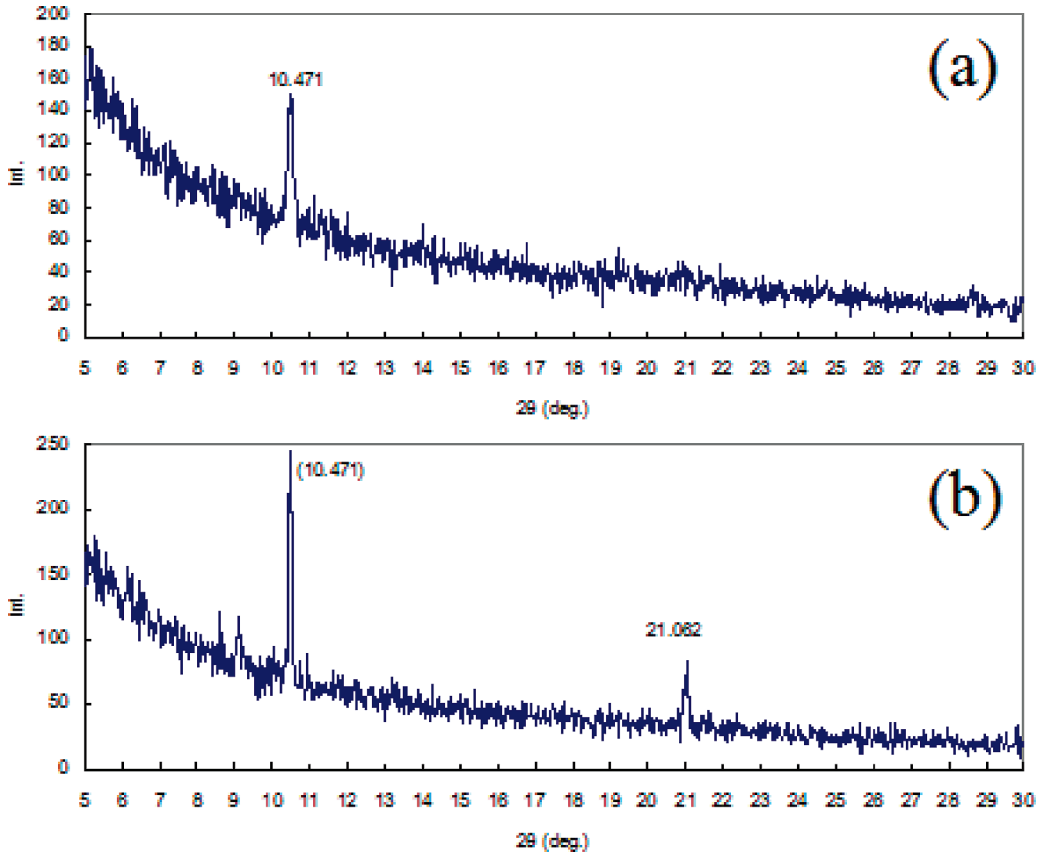

FIGURE 5. XRD of 45 nm TCDAHP on (a) 3 nm pentacene/NTS-SiO_2/Si and (b) 3 nm pentacene/r-NTS-SiO_2/Si surfaces.

are assigned as the (002) and (004) diffraction peaks, respectively, based on the calculated *d* spacing of 8.45 Å and a *c* axis of 17.11 Å for the unit cell. Thus, the crystallites have their *c* axis nearly perpendicular to the substrate surface. With this orientation, the $\pi-\pi$ stacking direction is nearly parallel to the substrate surface (Figure 6). The FET devices based on the TCDAHP films deposited on the pentacene buffer layer also showed significant improvement with rubbing treatment of the monolayer. With the TCDAHP film deposited on 3 nm pentacene/NTS-SiO_2/Si, a mobility of ~0.3 cm^2/(V s) was obtained in open air. With the film deposited on 3 nm pentacene/r-NTS/SiO_2/Si, the field-effect mobility was enhanced and exhibited anisotropy: ~1.4 cm^2/(V s) along the rubbing direction and ~0.7 cm^2/(V s) along the direction perpendicular to the rubbing direction. Figure 7 shows typical *I*−*V* characteristics of a device measured along the rubbing direction of the monolayer. Contribution of the pentacene buffer layer is ruled out or should be minimal because of the control experiments above (25).

Similar film deposition and device fabrication were prepared for TCDAP. An amorphous film was also obtained on SiO_2/Si and NTS/SiO_2/Si surfaces with no measurable field-effect mobility. When the film was deposited on a 3 nm pentacene buffer layer on NTS/SiO_2/Si and r-NTS/SiO_2/Si, respectively, p-type mobility was also observed. On the unrubbed NTS/SiO_2/Si surface, a mobility of 0.02−0.03 cm^2/(V s) was measured, whereas on the r-NTS/SiO_2/Si surface, a mobility of 0.10−0.13 cm^2/(V s) was obtained along the rubbing direction and 0.07 cm^2/(V s) was obtained in the direction perpendicular to the rubbing direction. Interestingly, the trend that TCDAHP is superior to TCDAP is in agreement with that of theoretical calculations based on the

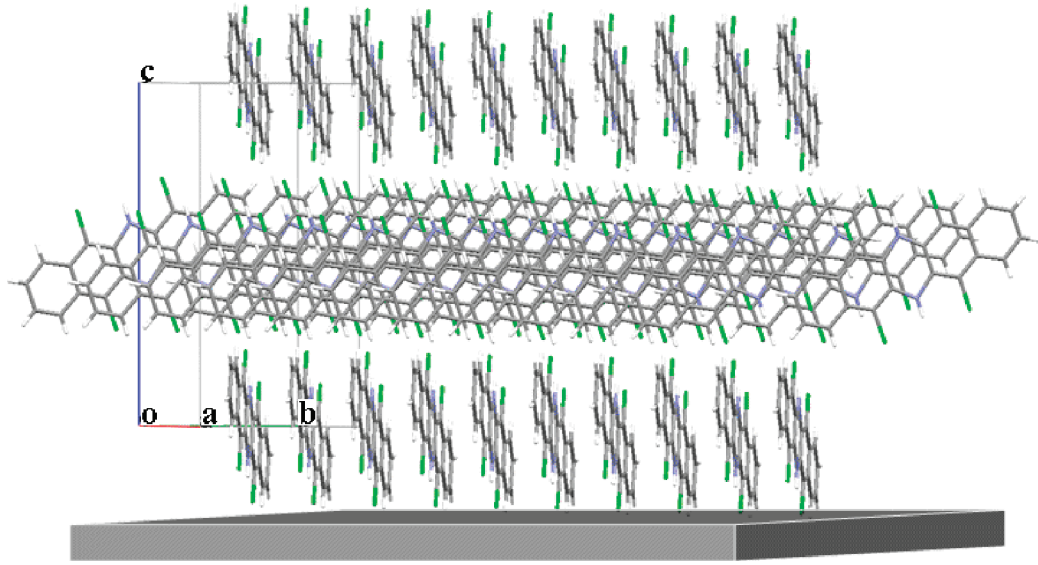

FIGURE 6. Schematic diagram showing the possible packing orientation of TCDAHP of "one grain" of the polycrystalline film based on the powder XRD and the unit cell length of the TCDAHP crystal.

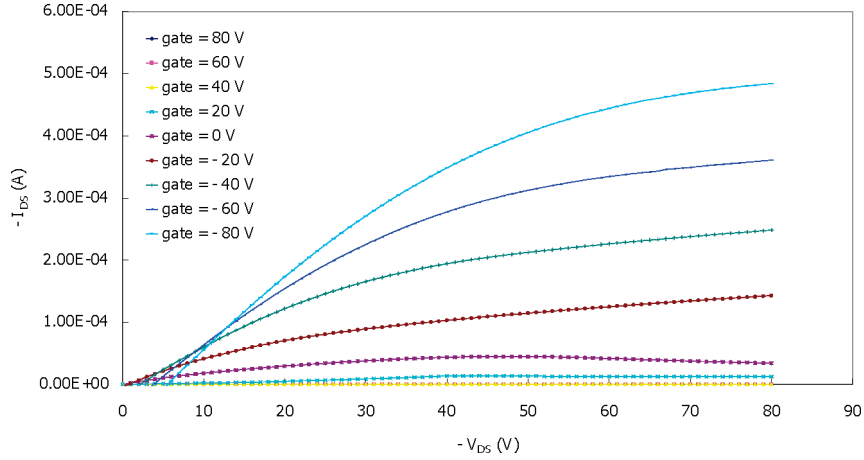

FIGURE 7. *I*−*V* characteristics of the TCDAHP film deposited on a pentacene/r-NTD/SiO_2/Si substrate, measured along the rubbing direction of the monolayer.

X-ray structures. The distinct difference between HOMOs of TCDAHP and TCDAP provides a possible explanation. The device appeared to be stable in that a similar mobility was measured after the device was left in ambient for 1 week.

CONCLUSION

In conclusion, two new semiconducting molecules were designed, synthesized, and assessed for their property as a channel material in p-type transistor application. With the introduction of four chlorine atoms at the 5, 7, 12, and 14 positions, both molecules crystallize into a shifted yet cofacial π−π stacking arrangement rather than a herringbone arrangement. In the very similar single-crystal coordinates, the cofacial packing results in high electronic coupling along the π−π stacking direction in the case of TCDAHP and low electronic coupling in the case of TCDAP, because of different MO distribution patterns in the HOMOs. The shifted π−π stacking also favors long needlelike crystal morphology, presumably due to faster crystal growth along the shorter axis of the unit cell, which coincides with the direction of π−π stacking. Such a growth pattern is, nevertheless, unfavorable for film formation. Deposition of TCDAHP on the SiO_2/Si or NTS-covered SiO_2/Si surface gave only amorphous films, and no mobility was measured. The noncrystallizing problem was, nevertheless, overcome with further surface modification using a 3 nm pentacene film as the buffer layer prepared on a NTS/SiO_2/Si substrate. The pentacene layer provides a surface with an ordered matrix of aromatic C−H bonds, which induces the formation of a crystalline film of TCDAHP. Further improvement in the crystallinity, grain size, and possibly connectivity of the grains was achieved with the pentacene buffer layer deposited on a prerubbed NTS/SiO_2/Si substrate. A high field-effect mobility of 1.4 cm^2/(V s) was obtained in air for the TCDAHP film on such a substrate surface. In contrast, the mobility for devices prepared from TCDAP on a similar pentacene buffer layer was 0.13 cm^2/(V s). This trend is the same as that evaluated theoretically based on the X-ray structures. This work provides a number of insights in the realization high mobility for an OFET: (1) while cofacial π−π stacking can be achieved by the careful design of the molecular framework, it may,

nevertheless, result in a dramatic growth rate difference in one of the dimensions (the $\pi-\pi$ stacking direction) of the crystal and jeopardize the film-forming property; (2) it is important for the detailed HOMO/LUMO topography to reach a high electronic coupling for otherwise similar crystal packings; (3) it is important for interfacial interaction between the substrate and molecules to induce crystallization, which is necessary for high mobility to be realized.

EXPERIMENTAL SECTION

Material Synthesis. 5,7,12,14-Tetrachloro-6,13-diaza-6,13-dihydropentacene (TCDAHP) was prepared from 6,13-diaza-6,13-dihydropentacene (9) by a slight modification of the procedure given in the literature (26). Thus, 6,13-diaza-6,13-dihydropentacene (1.12 g, 4.0 mmol) was suspended in carbon tetrachloride. Sulfuryl chloride (1.0 mL, 12.0 mmol) was added dropwise to the solution. The temperature was raised to 70 °C, and the reaction mixture was stirred on a water bath for 2 h. After cooling, water was slowly added to precipitate the product. The resulting solid, after filtration, was washed with acetone and dichloromethane and dried to give 844 mg (54%) of a greenish compound. The product was purified by sublimation. It is slightly soluble in solvents like $CHCl_3$, chlorobenzene, and CH_2Cl_2. ^{1}H NMR (400 MHz, $CDCl_3$): δ (ppm) 7.83 (dd, 4H, J_1 = 3.4 Hz, J_2 = 6.4 Hz), 7.33 (dd, 4H, J_1 = 3.4 Hz, J_2 = 6.4 Hz), 7.08 (s, 2H). EI MS: *m/z* 417.9 (M^+ monoisotopic, 78%), 419.9 ($M^+ + 2$, 100%). Elem anal. Calcd: C, 57.18; H, 2.40; Cl, 33.76; N, 6.67. Found: C, 57.35; H, 2.23; Cl, 33.90, N, 6.52.

6,13-Diazapentacene (DAP) was prepared from 6,13-diaza-6,13-dihydropentacene according to the literature (27) with the following modification. 6,13-Diaza-6,13-dihydropentacene (1.0 g) was suspended in warm pyridine, while 1.1 g of copper acetate monohydrate dissolved in pyridine was added to it. The reaction mixture immediately turned dark. The resulting mixture was heated on a water bath at 70 °C for about 8 h in open air. The mixture was cooled, flooded with water, washed several times with acetone, and dried. The resulting dark-green solid (0.8 g, 80%) was further purified by sublimation. DAP was found to be insoluble in most organic solvents. However, its ^{1}H NMR spectrum was determined by scanning for a long time. ^{1}H NMR (400 MHz, $CDCl_3$): δ (ppm) 8.92 (s, 4H), 8.07 (dd, 4H, J_1 = 2.9 Hz, J_2 = 6.9 Hz), 7.46 (dd, 4H, J_1 = 2.9 Hz, J_2 = 6.8 Hz). EI MS: *m/z* 280.1 (M^+, 100%).

5,7,12,14-Tetrachloro-6,13-diazapentacene (TCDAP) was prepared from DAP by a procedure similar to that in the preparation of TCDAHP. The crude solid was washed with acetone and dichloromethane and dried to afford 840 mg (51%) of grass-green compound TCDAP. The latter was found to be slightly soluble in solvents like $CHCl_3$, chlorobenzene, dimethyl sulfoxide, and CH_2Cl_2. ^{1}H NMR (400 MHz, $CDCl_3$): δ (ppm) 8.67 (dd, 4H, J_1 = 3.3 Hz, J_2 = 6.9 Hz), 7.69 (dd, 4H, J_1 = 3.3 Hz, J_2 = 6.9 Hz). EI MS: *m/z* 415.81 (M^+ monoisotopic, 67%), 417.81 ($M^+ + 2$, 100%). Elem anal. Calcd: C, 57.45; H, 1.93; Cl, 33.92; N, 6.70. Found: C, 57.76; H, 2.03; Cl, 33.59; N, 6.62.

Characterization. AFM analyses were carried out by using a Digital Instruments Multimode 3 atomic force microscope. Images were captured by a tapping mode with a silicon tip at 300 kHz frequency. The powder XRD was carried out by using the Philips X'Pert diffractometer with an X'Celerator detector. Cu Kα radiation at a power of 45 kV and 40 mA with a scanning step size of 0.008° was used.

Device Fabrication and Measurement. The highly *n*-doped silicon wafers, with a 300 nm thermally grown oxide layer, were cleaned by soaking in a 90 °C piranha solution [7:3 (v/v) concentrated H_2SO_4/30% H_2O_2], rinsed thoroughly with ultrahigh-purity water, and blown dry with a pure nitrogen flow. The NTS-covered silicon wafers (NTS-SiO_2/Si) were prepared by submersion into a 1% NTS solution in dry toluene for 3 min and rinsing with pure toluene. Rubbing of the monolayer was achieved by using a flannel cloth along a fixed direction as described previously (24). Thin films of TCDAHP (or TCDAP and the pentacene) were thermally evaporated under a vacuum of $1 \times {}^{-5}$ Torr and deposited on a SiO_2/Si or NTS-SiO_2/Si surface maintained at 55 °C. The film thickness was monitored with a quartz crystal microbalance, and the deposition was controlled at a rate of ~0.1 Å/s. FET devices were completed by evaporation of a 50-nm-thick gold source and drain electrodes on the organic films (top contact) through a shadow mask. The channel length (L) and width (W) are 50 and 500 μm, respectively. The electrical characteristics of the devices were measured under ambient conditions using a computer-controlled Agilent 4156C semiconductor parameter analyzer. The field-effect mobility of the OFET device was calculated from the saturation region according to eq 1,

$$I_{ds,sat} = (WC_i/2L)\mu_{sat}(V_{gs} - V_{th})^2 \quad (1)$$

where W and L are the channel width and length, respectively, C_i is the capacitance of the SiO_2 insulator, V_{gs} is the gate voltage, and V_{th} is the threshold voltage.

Computational Details. At high temperature (including room temperature), the charge carriers in the thin-film OFET are believed to be localized at individual molecules, and the charge-transport mechanism is a hopping mechanism that can be described by Marcus theory (11). The rate expression of a self-exchange process is

$$k_{et} = \frac{4\pi^2}{h}\frac{1}{\sqrt{4\pi\lambda k_B T}}t^2 \exp\left(-\frac{\lambda}{4k_B T}\right) \quad (2)$$

Because λ^+ values calculated at the B3LYP/6-31G** level have been shown to agree well with the experimental values from the gas-phase photoelectron spectrum (20, 28), λ^+ was estimated at the same level of theory. The total internal λ^+ is the sum of $\lambda_1{}^+$ and $\lambda_2{}^+$ (eqs 3–5).

$$\lambda^+ = \lambda_1{}^+ + \lambda_2{}^+ \quad (3)$$

$$\lambda_1{}^+ = E_+(Q_N) - E_+(Q_+) \quad (4)$$

$$\lambda_2{}^+ = E_N(Q_+) - E_N(Q_N) \quad (5)$$

$E_+(Q_N)$ is the total electronic energy of the cationic state in the neutral geometry, $E_+(Q_+)$ is the total energy of the cationic state in the cationic state geometry, $E_N(Q_+)$ is the total energy of the neutral state in the cationic state geometry, and $E_N(Q_N)$ is the total energy of the neutral state in the neutral geometry.

The electronic coupling t^+ was calculated according to eq 6 (11d):

$$t^+ = \frac{H_{RP} - S_{RP}(H_{RR} + H_{PP})/2}{1 - S_{RP}{}^2} \quad (6)$$

where H_{RP} is the charge-transfer integral, S_{RP} the spatial overlap, and H_{RR} and H_{PP} the site energies. All four terms are obtained via the direct coupling of localized monomer orbitals.

With λ^+ and t^+, one can calculate k_{et} according to eq 2. The diffusion coefficient D of charge carriers can then be given by the Einstein−Smoluchowski equation (eq 7) (29), where L is the effective length of the electron transfer (approximated by the molecular center-to-center distance of a dimer). This allows us to evaluate the drift mobility of the charge from the Einstein relation (29), as shown in eq 8, where e is the electronic charge, k_B is the Boltzmann constant, and T is the temperature in Kelvin (300 K in this study). This method and its variations have been employed for the theoretical predictions of the charge-carrier mobility of organic semiconductors (15, 16b, 21).

$$D = L^2 k_{et}/2 \tag{7}$$

$$\mu = eD/k_B T \tag{8}$$

Gaussian 03 (30) is used to calculate EA, IP, and λ^+ values at the B3LYP/6-31G** level of theory, while the Amsterdam density functional program (31) is employed to obtain H_{RP}, S_{RP}, H_{RR}, and H_{PP} (32) for estimating the electronic couplings (t^+) at the PW91/DZP level of theory (the local density functional VWN in conjunction with the PW91 gradient corrections). λ^+'s are estimated based on the optimized molecular structures ($\langle S^2 \rangle$ of the charged states is in the range of 0.7576−0.7661), and the t^+'s are calculated on the basis of the X-ray structures.

Acknowledgment. The authors thank the National Science Council, Taiwan, Republic of China, and Academia Sinica for financial support. The computing time granted by the National Center for High-Performance Computing and the Computing Center of Academia Sinica is acknowledged.

REFERENCES AND NOTES

(1) http://www.sony.jp/products/Consumer/oel/products/index.html.
(2) (a) Jang, J. *Mater. Today* **2006**, *9*, 46. (b) http://www.engadget.com/2005/07/13/fujitsus-flexible-low-power-color-screen/. (c) http://www.eink.com/technology/flexible.html.
(3) (a) Klauk, H.; Halik, M.; Zschieschang, U.; Schmid, G.; Radlik, W.; Weber, W. *J. Appl. Phys.* **2002**, *92*, 5259. (b) Kelley, T. W.; Boardman, L. D.; Dunbar, T. D.; Muyres, D. V.; Pellerite, M. J.; Smith, T. P. *J. Phys. Chem. B* **2003**, *107*, 5877. (c) Kelley, T. W.; Muyres, D. V.; Baude, P. F.; Smith, T. P.; Jones, T. D. *Mater. Res. Soc. Symp. Proc.* **2003**, *771*, L6.5.
(4) (a) Lewis, I.; Singer, L. *J. Phys. Chem.* **1981**, *85*, 354. (b) Briks, J.; Appleyard, J.; Pope, R. *Photochem. Photobiol.* **1963**, *2*, 493. (c) Clar, E. *Polycyclic Aromatic Hydrocarbons*; Academic Press: London, 1964; Vol. 1. (d) Maliakal, A.; Raghavachari, K.; Katz, H.; Chandross, E.; Siegrist, T. *Chem. Mater.* **2004**, *16*, 4980.
(5) (a) Anthony, J. E. *Chem. Rev.* **2006**, *106*, 5028. (b) Miao, Q.; Chi, X.; Xiao, S.; Zeis, R.; Lefenfeld, M.; Siegrist, T.; Steigerwald, M. L.; Nuckolls, C. *J. Am. Chem. Soc.* **2006**, *128*, 1340.
(6) (a) Miao, S.; Brombosz, S. M.; Schleyer, P. v. R.; Wu, J. I.; Barlow, S.; Marder, S. R.; Hardcastle, K. I.; Bunz, U. H. F. *J. Am. Chem. Soc.* **2008**, *130*, 7339. (b) Gao, B.; Wang, M.; Cheng, Y.; Wang, L.; Jing, X.; Wang, F. *J. Am. Chem. Soc.* **2008**, *130*, 8297.
(7) (a) Winkler, M.; Houk, K. N. *J. Am. Chem. Soc.* **2007**, *129*, 1805. (b) Chen, H.-Y.; Chao, I. *ChemPhysChem* **2006**, *7*, 2003.
(8) Di, C.-a.; Li, J.; Yu, G.; Xiao, Y.; Guo, Y.; Liu, Y.; Qian, X.; Zhu, D. *Org. Lett.* **2008**, *10*, 3025.
(9) (a) Miao, Q.; Nguyen, T.-Q.; Someya, T.; Blanchet, G. B.; Nuckolls, C. *J. Am. Chem. Soc.* **2003**, *125*, 10284. (b) Wu, J. I.; Wannere, C. S.; Mo, Y. R.; Schleyer, P. V.; Bunz, U. H. F. *J. Org. Chem.* **2009**, *74*, 4343.
(10) (a) Tang, Q.; Zhang, D. Q.; Wang, S. L.; Ke, N.; Xu, J. B.; Yu, J. C.; Miao, Q. *Chem. Mater.* **2009**, *21*, 1400. (b) Tang, Q.; Liu, J.; Chan, H. S.; Miao, Q. *Chem.—Eur. J.* **2009**, *15*, 3965.
(11) (a) Marcus, R. A. *Rev. Mod. Phys.* **1993**, *65*, 599. (b) Barbara, P. F.; Meyer, T. J.; Ratner, M. A. *J. Phys. Chem.* **1996**, *100*, 13148. (c) da Silva Filho, D. A.; Olivier, Y.; Coropceanu, V.; Brédas, J.-L.; Cornil, J. Theoretical Aspects of Charge Transport in Organic Semiconductors: A Molecular Perspective. In *Organic Field-Effect Transistors*; Bao, Z., Locklin, J., Eds.; CRC: Boca Raton, FL, 2007; Chapter 1. (d) Coropceanu, V.; Cornil, J.; da Silva Filho, D. A.; Olivier, Y.; Silbey, R.; Brédas, J.-L. *Chem. Rev.* **2007**, *107*, 926. (e) Cornil, J.; Brédas, J.-L.; Zaumseil, J.; Sirringhaus, H. *Adv. Mater.* **1007**, *19*, 1791. (f) Troisi, A. *Adv. Mater.* **2007**, *19*, 2000.
(12) (a) Brédas, J.-L.; Calbert, J. P.; da Silva Filho, D. A.; Cornil, J. *Proc. Natl. Acad. Sci. U.S.A.* **2002**, *99*, 5804. (b) Brédas, J.-L.; Beljonne, D.; Coropceanu, V.; Cornil, J. *Chem. Rev.* **2004**, *104*, 4971. (c) Haddon, R. C.; Chi, X.; Itkis, M. E.; Anthony, J. E.; Eaton, D. L.; Siegrist, T.; Mattheus, C. C.; Palstra, T. T. M. *J. Phys. Chem. B* **2002**, *106*, 8288.
(13) Sarma, J. A. R. P.; Desiraju, G. R. *Acc. Chem. Res.* **1986**, *19*, 222.
(14) Moon, H.; Zeis, R.; Borkent, E.-J.; Besnard, C.; Lovinger, A. J.; Siegrist, T.; Kloc, C.; Bao, Z. *J. Am. Chem. Soc.* **2004**, *126*, 15322.
(15) Cornil, J.; Lemaur, V.; Calbert, J.-P.; Brédas, J.-L. *Adv. Mater.* **2002**, *14*, 726.
(16) (a) Chen, H.-Y.; Chao, I. *Chem. Phys. Lett.* **2005**, *401*, 539. (b) Kuo, M.-Y.; Chen, H.-Y.; Chao, I. *Chem.—Eur. J.* **2007**, *13*, 4750.
(17) Laquindanum, J. G.; Katz, H. E.; Lovinger, A. J.; Dodabalapur, A. *Adv. Mater.* **1997**, *9*, 36.
(18) Dimitrakopoulos, C. D.; Malenfant, P. R. L. *Adv. Mater.* **2002**, *14*, 99.
(19) Weng, S. Z.; Hu, W. S.; Kuo, C. H.; Tao, Y. T.; Fan, L. J.; Yang, Y. W. *Appl. Phys. Lett.* **2006**, *89*, 172103.
(20) Kwon, O.; Coropceanu, V.; Gruhn, N. E.; Durivage, J. C.; Laquindanum, J. G.; Katz, H. E.; Cornil, J.; Brédas, J. L. *J. Chem. Phys.* **2004**, *120*, 8186.
(21) (a) Song, Y.; Di, C.; Yang, X.; Li, S.; Xu, W.; Liu, Y.; Yang, L.; Shuai, Z.; Zhang, D.; Zhu, D. *J. Am. Chem. Soc.* **2006**, *128*, 15940. (b) Valiyev, F.; Hu, W.-S.; Chen, H.-Y.; Kuo, M.-Y.; Chao, I.; Tao, Y. T. *Chem. Mater.* **2007**, *19*, 3018. (c) Chang, Y.-C.; Chen, Y.-D.; Chen, C.-H.; Wen, Y.-S.; Lin, J.-T.; Chen, H.-Y.; Kuo, M.-Y.; Chao, I. *J. Org. Chem.* **2008**, *73*, 4608. (d) Van Vooren, A.; Kim, J.-S.; Cornil, J. *ChemPhysChem* **2008**, *9*, 989. (e) Zhang, Y.; Cai, X.; Bian, Y.; Li, X.; Jiang, J. *J. Phys. Chem. C* **2008**, *112*, 5148. (f) Yang, X.; Li, Q.; Shuai, Z. *Nanotechnology* **2007**, *18*, 424029. (g) Yang, X.; Wang, L.; Wang, C.; Long, W.; Shuai, Z. *Chem. Mater.* **2008**, *20*, 3205.
(22) Kim, D. H.; Lee, H. S.; Yang, H.; Yang, L.; Cho, K. *Adv. Funct. Mater.* **2008**, *18*, 1363.
(23) (a) Itaka, K.; Yamashiro, M.; Yamaguchi, J.; Haemori, M.; Yaginuma, S.; Matsumoto, Y.; Kondo, M.; Koinuma, H. *Adv. Mater.* **2006**, *18*, 1713. (b) Haemori, M.; Yamaguchi, J.; Yaginuma, S.; Itaka, K.; Koinuma, H. *Jpn. J. Appl. Phys.* **2005**, *Part 1*, 44–3740. (c) Seo, J. H.; Park, D. S.; Cho, S. W.; Kim, C. Y.; Jang, W. C.; Whang, C. N.; Yoo, K.-H.; Chang, G. S.; Pedersen, T.; Moewes, A.; Chae, K. H.; Cho, S. J. *Appl. Phys. Lett.* **2006**, *89*, 163505.
(24) Hu, W. S.; Weng, S. Z.; Tao, Y. T.; Liu, H. J.; Lee, H. Y. *Org. Electron.* **2008**, *9*, 385.
(25) It is noted that, under some special deposition conditions, such as supersonic molecular beam deposition (Asadi, K.; et al. *Adv. Mater.* **2009**, *21*, 1), a single layer of pentacene with contacting islands or full coverage can be prepared and finite mobility can be measured [in the range of 0.015 $cm^2/(V\ s)$]. In our deposition conditions, discontinuous islands of three to four layers were obtained. The contribution of the pentacene buffer layer, if any, should be lower than the low mobility obtained using the same pentacene buffer layer. For example, TCDAP in this work gave 0.1 $cm^2/(V\ s)$ under such conditions.
(26) Van Allan, J. A.; Adel, R. E.; Reynolds, G. A. *J. Org. Chem.* **1963**, *28*, 520.
(27) Van Allan, J. A.; Adel, R. E.; Reynolds, G. A. *J. Org. Chem.* **1962**, *27*, 2873.
(28) (a) Gruhn, N. E.; da Silva Filho, D. A.; Bill, T. G.; Malagoli, M.; Coropceanu, V.; Kahn, A.; Brédas, J.-L. *J. Am. Chem. Soc.* **2002**, *124*, 7918. (b) Coropceanu, V.; Malagoli, M.; da Silva Filho, D. A.; Gruhn, N. E.; Bill, T. G.; Brédas, J.-L. *Phys. Rev. Lett.* **2002**, *89*, 275503.
(29) Atkins, P. W. *Physical Chemistry*, 5th ed.; Oxford University Press: Oxford, U.K., 1994.
(30) Frisch, M. J.; Trucks, G. W.; Schlegel, H. B.; Scuseria, G. E.; Robb, M. A.; Cheeseman, J. R.; Montgomery, J. A.; Vreven, T., Jr.; Kudin, K. N.; Burant, J. C.; Millam, J. M.; Iyengar, S. S.; Tomasi, J.; Barone, V.; Mennucci, B.; Cossi, M.; Scalmani, G.; Rega, N.; Petersson, G. A.; Nakatsuji, H.; Hada, M.; Ehara, M.; Toyota, K.; Fukuda, R.;

Hasegawa, J.; Ishida, M.; Nakajima, T.; Honda, Y.; Kitao, O.; Nakai, H.; Klene, M.; Li, X.; Knox, J. E.; Hratchian, H. P.; Cross, J. B.; Bakken, V.; Adamo, C.; Jaramillo, J.; Gomperts, R.; Stratmann, R. E.; Yazyev, O.; Austin, A. J.; Cammi, R.; Pomelli, C.; Ochterski, J. W.; Ayala, P. Y.; Morokuma, K.; Voth, G. A.; Salvador, P.; Dannenberg, J. J.; Zakrzewski, V. G.; Dapprich, S.; Daniels, A. D.; Strain, M. C.; Farkas, O.; Malick, D. K.; Rabuck, A. D.; Raghavachari, K.; Foresman, J. B.; Ortiz, J. V.; Cui, Q.; Baboul, A. G.; Clifford, S.; Cioslowski, J.; Stefanov, B. B.; Liu, G.; Liashenko, A.; Piskorz, P.; Komaromi, I.; Martin, R. L.; Fox, D. J.; Keith, T.; Al-Laham, M. A.; Peng, C. Y.; Nanayakkara, A.; Challacombe, M.; Gill, P. M. W.; Johnson, B.; Chen, W.; Wong, M. W.; Gonzalez, C.; Pople, J. A. *Gaussian 03*, revision D.02; Gaussian, Inc.: Wallingford, CT, 2004.

(31) (a) te Velde, G.; Bickelhaupt, F. M.; Baerends, E. J.; Fonseca Guerra, C.; van Gisbergen, S. J. A.; Snijders, J. G.; Ziegler, T. *J. Comput. Chem.* **2001**, *22*, 931. (b) Fonseca Guerra, C.; Snijders, J. G.; te Velde, G.; Baerends, E. J. *Theor. Chem. Acc.* **1998**, *99*, 391. (c) *ADF2007.01, SCM, Theoretical Chemistry*; Vrije Universiteit: Amsterdam, The Netherlands, http://www.scm.com.

(32) (a) Senthilkumar, K.; Grozema, F. C.; Buckelhaupt, F. M.; Siebbeles, L. D. A. *J. Chem. Phys.* **2003**, *119*, 9809. (b) Prins, P.; Senthilkumar, K.; Grozema, F. C.; Jonkheijm, P.; Schenning, A. P. H. J.; Meijer, E. W.; Siebbeles, L. D. A. *J. Phys. Chem. B* **2005**, *109*, 18267.

AM9004418